Since January 2020 Elsevier has created a COVID-19 resource centre with free information in English and Mandarin on the novel coronavirus COVID-19. The COVID-19 resource centre is hosted on Elsevier Connect, the company's public news and information website.

Life Sciences 308 (2022) 120930

Contents lists available at ScienceDirect

Life Sciences

journal homepage: www.elsevier.com/locate/lifescie

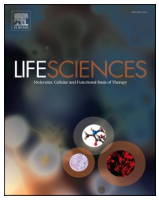

SARS-CoV-2 infection and replication kinetics in different human cell types: The role of autophagy, cellular metabolism and ACE2 expression

Cynthia Silva Bartolomeo [a,b,1], Robertha Mariana Rodrigues Lemes [c,d,1], Rafael Leite Morais [j], Gabriela Cruz Pereria [f], Tamires Alves Nunes [b], Angelica Jardim Costa [g], Rui Monteiro de Barros Maciel [c,e], Carla Torres Braconi [h], Juliana Terzi Maricato [h], Luiz Mario Ramos Janini [h], Liria Hiromi Okuda [i], Kil Sun Lee [f], Carla Máximo Prado [b,2], Rodrigo Portes Ureshino [c,d,2], Roberta Sessa Stilhano [a,2,*]

[a] Department of Physiological Sciences, Faculdade de Ciências Médicas da Santa Casa de São Paulo, São Paulo, SP, Brazil
[b] Department of Biosciences, Universidade Federal de São Paulo, Santos, SP, Brazil
[c] Department of Biological Sciences, Universidade Federal de São Paulo, Diadema, SP, Brazil
[d] Laboratory of Molecular and Translational Endocrinology, Escola Paulista de Medicina, Universidade Federal de São Paulo, São Paulo, SP, Brazil
[e] Department of Medicine, Escola Paulista de Medicina, Universidade Federal de São Paulo, São Paulo, SP, Brazil
[f] Department of Biochemistry, Escola Paulista de Medicina, Universidade Federal de São Paulo, São Paulo, SP, Brazil
[g] Department of Pharmacology, Escola Paulista de Medicina, Universidade Federal de São Paulo, São Paulo, SP, Brazil
[h] Department of Microbiology Immunology and Parasitology, Escola Paulista de Medicina, Universidade Federal de São Paulo, São Paulo, SP, Brazil
[i] Instituto Biológico, Secretaria de Agricultura e Abastecimento, São Paulo, SP, Brazil
[j] Department of Biophysics, Escola Paulista de Medicina, Universidade Federal de São Paulo, São Paulo, Brazil

ARTICLE INFO

Keywords:
COVID-19
ACE2
TMPRSS2
Cell lines
Mitochondria
Autophagy

ABSTRACT

Aims: This study evaluated SARS-CoV-2 replication in human cell lines derived from various tissues and investigated molecular mechanisms related to viral infection susceptibility and replication.
Main methods: SARS-CoV-2 replication in BEAS-2B and A549 (respiratory tract), HEK-293 T (kidney), HuH7 (liver), SH-SY5Y (brain), MCF7 (breast), Huvec (endothelial) and Caco-2 (intestine) was evaluated by RT-qPCR. Concomitantly, expression levels of ACE2 (Angiotensin Converting Enzyme) and TMPRSS2 were assessed through RT-qPCR and western blot. Proteins related to autophagy and mitochondrial metabolism were monitored in uninfected cells to characterize the cellular metabolism of each cell line. The effect of ACE2 overexpression on viral replication in pulmonary cells was also investigated.
Key findings: Our data show that HuH7, Caco-2 and MCF7 presented a higher viral load compared to the other cell lines. The increased susceptibility to SARS-CoV-2 infection seems to be associated not only with the differential levels of proteins intrinsically related to energetic metabolism, such as ATP synthase, citrate synthase, COX and NDUFS2 but also with the considerably higher TMPRSS2 mRNA expression. The two least susceptible cell types, BEAS-2B and A549, showed drastically increased SARS-CoV-2 replication capacity when ACE2 was overexpressed. These modified cell lines are relevant for studying SARS-CoV-2 replication in vitro.
Significance: Our data not only reinforce that TMPRSS2 expression and cellular energy metabolism are important molecular mechanisms for SARS-CoV-2 infection and replication, but also indicate that HuH7, MCF7 and Caco-2 are suitable models for mechanistic studies of COVID-19. Moreover, pulmonary cells overexpressing ACE2 can be used to understand mechanisms associated with SARS-CoV-2 replication.

* Corresponding author at: 61 Dr. Cesário Mota Junior Street, São Paulo, SP Zipcode 01221-020, Brazil.
E-mail address: roberta.yamaguchi@fcmsantacasasp.edu.br (R.S. Stilhano).
[1] Joint first authors.
[2] Joint senior # authors.

https://doi.org/10.1016/j.lfs.2022.120930
Received 1 June 2022; Received in revised form 29 August 2022; Accepted 31 August 2022
Available online 6 September 2022

1. Introduction

COVID-19, caused by SARS-CoV-2, has emerged as a life-changing pandemic, impacting global health and affecting economies and societies. As of August 2022, about 600 million people worldwide had been reportedly infected with the virus during the current pandemic (data from Johns Hopkins in August/2022). COVID-19 is classified as an airborne disease, but alternative paths of transmission include the direct contact of the lips, nose or eyes with the infectious droplets [1]. SARS-CoV-2 can replicate in the lower respiratory tract and patients may develop acute respiratory distress syndrome (ARDS) [2]. In some cases, extrapulmonary effects are also observed such as diarrhea, cardiac arrhythmias, kidney and liver injury, rhabdomyolysis, sarcopenia, coagulopathy, neurological symptoms and shock [2,3]. Studies have shown that the most prevalent comorbidities in COVID-19 patients were hypertension and diabetes, followed by cardiovascular diseases. Also, they are more susceptible to developing a severe form of COVID-19 and usually exhibit a poor prognosis [4,5].

The main viral target in host cells is ACE2 (Angiotensin-converting enzyme 2) and TMPRSS2 (Transmembrane protease, serine 2). ACE2 is the host receptor that interacts with the spike protein presented in the virus envelope. The spike protein is formed by two subunits: S1 (interacts with ACE2) and S2 (mediates the fusion). There is a furin cleavage motif between the subunits, which is cleaved by the host cell. When the virus binds to ACE2, the spike is cleaved by the transmembrane serine protease TMPRSS2 at the S2′ site. This cleavage allows the S2 subunit fusion with the host bilayer releasing the virus RNA into the cell. Some cells don't express TMPRSS2 or the expression is too low. So, the virus enters in the cell through the endosomal pathway, using ACE2 and cathepsins [2]. Once inside the cells, SARS-CoV-2 hijacks protein production machinery through cross-talk with autophagic machinery [6] and mitochondrial metabolism [7] for its replication.

The invasion and replication of SARS-CoV-2 have been evaluated in several cell lines such as BEAS-2B, A549 and Calu-3 (respiratory tract), HEK-293 T (kidney), HuH7 (liver), SH-SY5Y (brain), Caco-2 (intestine), Huvec (endothelium) and Vero-E6 (monkey kidney cell line), but viral loads were cell-type dependent. It is plausible that this distinct susceptibility is due to differential ACE2 and TMPRSS2 expression in various organs.

According to the GTEx database, the terminal ileum expresses the highest levels of *ACE2* in the human body, followed by the breast, colon and kidneys (https://gtexportal.org/home/gene/ACE2 - ENSG00000130234.10). Additionally, TMPRSS2 expression is highest in the prostate, colon, breast, stomach, kidney, lungs and liver. (https://gtexportal.org/home/gene/ACE2 - ENSG00000184012.11). Due to constitutive ACE2 expression throughout the body, several cell lines were used to study the viral cycle and its effects on cell biology.

Among the various cell lines, kidney (Vero E6 and HEK-293), liver (HuH7), intestinal (Caco-2) and respiratory tract (Calu-3) cells have been employed as already-in-use cell models, as described in the systematic review of Kumar et al. (2021) [8]. Indeed, the characterization of cell lines derived from different organs and systems affected by SARS-CoV-2 is highly relevant for research and clinical advances.

Thus, the present study evaluated viral entrance and replication in different cell lines to identify relationships between the SARS-CoV-2 infection/replication rates and the expression of proteins related to autophagy and mitochondrial metabolism, ACE2 and TMPRRS2. As far as we know, this is the first study to simultaneously compare the SARS-CoV-2 infection and replication in multiple cell lines.

2. Materials and methods

2.1. Cell cultures

A panel composed of the A549 (human lung adenocarcinoma), BEAS-2B (immortalized bronchial epithelial cell line), Caco-2 (colorectal adenocarcinoma cell line), HEK-293 T (immortalized renal epithelial cell line), HuH7 (hepatocarcinoma cell line), HUVEC (endothelial cell derived from the immortalized umbilical vein), MCF7 (cell derived from breast carcinoma) and SH-SY5Y (neuroblastoma cell line) human cell lines was monitored during in vitro SARS-CoV-2 infection. The Vero E6 cell line (cells derived from primate renal epithelium) was used in parallel as a comparative viral expansion and behavior model and utilized in other viral infection protocols [9]. All strains were cultivated and expanded in DMEM/F12 culture medium with 10 % FBS (fetal bovine serum) at 37 °C in an atmosphere of 5 % CO_2. The wells of the plates for BEAS-2B cultures were pretreated with type I collagen according to the manufacturer's instructions (Thermo Fisher, Waltham, Massachusetts, USA). All procedures were approved by the Institutional Ethics Committee (#6864310320 CEP-UNIFESP).

2.2. Kinetics of SARS-CoV-2 internalization and replication

The SARS-CoV-2 virus was obtained from a nasopharyngeal sample isolated from a Brazilian patient (EPI_ISL_413016) and donated by Prof. Edison Durigon and Paolo Zanotto (University of São Paulo) and José Luiz Proença Módena (State University of Campinas). The strain sequence was deposited in GenBank (MT 126808). After isolation, SARS-CoV-2 was amplified in the fourth passage in Vero E6 cells at a titer of 5×10^7 plaque-forming units (PFU/mL) after the plaque assay [10], which contributes to estimation of the infectivity capacity of the virus.

For the in vitro infection protocol, 1×10^5 cultured BEAS-2B, A549, Caco-2, HEK-293 T, HuH7, HUVEC, MCF7, SH-SY5Y and Vero E6 cells were infected with SARS-CoV-2 at a 0.2 estimated MOI (multiplicity of infection) for 2 h in DMEM-F12 medium supplemented with 1 % FBS under standard conditions (5 % CO_2, 37 °C) [11]. After incubation with SARS-CoV-2, the supernatants were removed, and the adhered cells were washed with PBS before extraction of the total RNA with the RNeasy Mini Kit, following the manufacturer's recommendations (Qiagen, Hilden, Germany). Additionally, following the same infection strategy as the internalization assay, after 2 h of infection and washing the cells with PBS, the replication kinetics of all strains were monitored by additional incubation for 24, 48, 72 or 96 h in DMEM-F12 medium supplemented with 10 % FBS under standard conditions. For mock controls, the same volume of DMEM/F12 culture medium was added to each kinetic experiment, and the same procedures were followed. At the end of each incubation period, the plated cells and the supernatants were collected, and the total RNA was extracted and processed using the RNeasy Mini Kit (Qiagen) and Quick RNA viral kit (Zymo Research, Irvine, California, USA), respectively. The same protocol and reagents published in Lemes et al. (2021) were used for viral detection [12]. All experiments with virus were performed in a biosafety level 3 laboratory (BLS3), in accordance with WHO recommendations and under the laboratory biosafety guidance required for the SARS-CoV-2 at the BLS3 facilities at the Federal University of São Paulo and the Biological Institute of São Paulo.

2.3. Gene expression of ACE2 and TMPRSS2 by RT-qPCR

ACE2 and *TMPRSS2* expression levels were evaluated by RT-qPCR. Briefly, the mRNA extracted with the RNeasy Mini Kit in the cell kinetics assays during SARS-CoV-2 infection of all the strains was quantified spectrophotometrically using a NanoDrop device (Thermo Fisher) and transcribed into cDNA with the High-Capacity kit, according to the manufacturer's instructions (Thermo Fisher). The cDNA obtained was subjected to the RT-qPCR reaction, together with the SYBR-Green reagent (Qiagen) and primer pairs for human ACE2 (ACE2_FW: 5′-CAT TGG AGC AAG TGT TGG ATC TT-3′ ACE2_RV: 5′-GAG CTA ATG CAT GCC ATT CTC A-3′), or for human TMPRSS2 (TMPRSS2_FW 5′-TAG AGA GCA GCA TTC CCA GG-3′ TMPRSS2_RV 5′-TAA GAA GGG GCA ATA AAG AAG-3′), primate ACE2 (ACE2_FW: 5'-CAT TGG AGC AAG TGT TGG ATC TT-3′; ACE2_RV: 5′-GAG CTA ATG CAT GCC ATT CTC A-3′);

primate TMPRSS2 (TMPRSS2_FW: 5′-CTC TAA CTG GTG CGA TGG CG-3′; TMPRSS2_RV: 5'-TGC CAG GAC TTC CTC TGA GAT G-3′) and ROX. The reactions were carried out on an Applied 7500 RT-PCR machine (Applied Biosystems, Waltham, Massachusetts, USA). The analysis was performed by the relative comparison method ($2^{-\Delta\Delta CT}$), and the samples were compared with the endogenous *RPL35* expression (primers: RPL35-FW 5′-CGA GTC GTC CGG AAA TCC AT-3′; RPL35-RV 5′-GGC TTG TAC TTC TTG CCC TTG-3′).

2.4. Western blotting

For the analysis of ACE2 and TMPRSS2 protein expression, 5×10^5 cells (BEAS-2B, A549, Caco-2, HEK-293 T, HuH7, HUVEC, MCF7, SH-SY5Y and Vero E6) were cultivated for 48 h in DMEM-F12 supplemented with 10 % FBS, under standard conditions (5 % CO_2, 37 °C). After incubation, supernatants were discarded, and adhered cells were washed with PBS. Cells were lysed with RIPA lysis buffer (150 mM NaCl; 1 % NP-40; 0.5 % deoxycholic acid; 0.1 % SDS; 50 mM Tris pH 8.0; 0.2 mM $MgCl_2$) and protease inhibitors. Total protein was extracted and quantified using a BCA kit (Thermo Fisher). Then, 20 μg of total protein from each strain were separated on 12 % or 7.5 % SDS-PAGE gels (according to the molecular weight of the protein of interest) and transferred to PVDF membranes.

Ponceau staining (0.1 %) was used to monitor the protein equivalents among all cell lysates (Fig. S1). Then, the membranes were blocked with 5 % bovine serum albumin (BSA) and incubated overnight at 4 °C with the primary antibody to the protein of interest (ACE2- ABCAM 'ab108252'; ATP5H- ABCAM 'ab173006'; Caspase-3- ABCAM 'ab32351'; Cathepsin- L- Santa Cruz 'sc-32320'; Citrate Synthase- Cell Signaling '14309'; Cytochrome c oxygenase 2 (cox)- Proteintech '55,070-I-AP'; LAMP-1- Santa Cruz '20011'; LC3B- Cell Signaling '2775'; NDUFS2- ABCAM 'ab192022' or TMPRSS2 - Santa Cruz 'sc515727'). The blots were then incubated with secondary antibodies labeled with horseradish peroxidase (HRP, Thermo Fisher). The blots were developed with ECL (Perkin Elmer, Waltham, Massachusetts, USA), and luminescence was recorded with a UVITEC digital photo documentation system (UVITEC Cambridge, Cambridge, Cambridgeshire, UK). Some membranes were stripped with Restore Plus Blot Buffer (Thermo Fisher) and processed again with a different primary antibody. The images were analyzed by densitometry using the Image J software (NIH, Bethesda, MD, USA), and data are presented as percentages, considering the sum of all densitometry values of each protein as 100 %.

2.5. Assessment of viability, proliferation and morphology of cell profiles

For the cell viability and morphology analyses during the infection kinetics by SARS-CoV-2, 1×10^5 of cultured BEAS-2B, A549, Caco2, Hek293T, Huh7, HUVEC, MCF7, SH-SY5Y and Vero E6 cells were infected or not (Mock) with SARS-CoV-2 at 0.2 MOI for 2 h in DMEM-F12 supplemented with 1 % FBS under standard conditions (5 % CO_2, 37 °C). After incubation, supernatants were removed, and cells were washed with PBS and incubated again for 24, 48, 72, or 96 h in DMEM-F12 supplemented with 10 % FBS under standard conditions. At the end of each incubation, the cells were incubated with 5 mg/mL MTT reagent (Sigma) for the cell viability assay or fixed with 4 % PFA-paraformaldehyde for cell morphology analyses.

The cell viability analyses involved dissolving the derived formazan in 100 % DMSO and measuring the absorbance of the suspension at 590 nm in a spectrophotometer. For the cell morphology analyses, the profile of each infected cell line was compared to its respective control (Mock). Images were captured with a Zeiss Primo Verti (Oberkochen, Germany) microscope using a 20× objective under a brightfield. Lastly, for the proliferation assays, cells were followed up over 5 days, at 1, 24, 48, 72 and 96 h. The doubling of each lineage cell was monitored through visual observations, and cell counting was performed under the same conditions as the morphology assay.

2.6. ACE2 enzymatic activity assay

ACE2 activity was evaluated as previously described but with some modifications [13]. We cultivated 5×10^5 BEAS-2B, BEAS-2B-ACE2, A549, A549-ACE2 Caco2, HEK-293T, HuH7, HUVEC, MCF7, SH-SY5Y or Vero E6 cells, in DMEM-F12 supplemented with 10 % FBS under standard conditions (5 % CO_2, 37 °C) for 48 h. After incubation, supernatants were discarded, adhered cells were washed with PBS, and total protein was extracted following cell lysis in RIPA buffer without protease inhibitors. The reaction occurs by the hydrolysis of the substrate MCA-Ala-Pro-Lys (Dnp)-OH and is expressed in arbitrary fluorescence units (AFUs) in μM/min/μg protein. Herein, 20 μL of protein extract from each cell line were incubated with buffer (50 mM HEPES-NaOH, 200 mM NaCl, 10 mM $ZnCl_2$, pH 6.8) and 50 mM MCA-Ala-Pro-Lys (Dnp)-OH substrate (Aminotech, Diadema, Sao Paulo, Brazil) at 37 °C subsequently sturred for 40 min. The ACE2 activity was assessed by measuring fluorescence ($\lambda_{EX} = 320$ nm and $\lambda_{EM} = 430$ nm) attributed to MCA-Ala-Pro-Lys (Dnp)-OH hydrolysis. Fluorescence was detected and analyzed using a Synergy H1 spectrofluorometer (Biotek, Winooski, Vermont, USA). MLN-4760 (Sigma-Aldrich, San Luis, Missouri, USA) was used as a specific inhibitor of ACE2 activity at 10 μM. The fluorescence parameter was defined as AFUs.

2.7. Enzyme-linked immunosorbent assay

ACE2 protein content was measured in samples of cells (wild-type or ACE2 positive), lysed with RIPA lysis buffer, using the Human ACE2 DuoSet ELISA Kit (R&D Systems, Minneapolis, Minnesota, USA) according to the manufacturer's recommendations. The wild-type samples were measured at a dilution of 1:10, and ACE2 positive cell samples were diluted at 1:100. Data are expressed in pg/mL after analysis and dilution correction.

2.8. ACE2 overexpression

ACE2 protein overexpression was performed in BEAS-2B and A549 cells by nucleofection with pCEP4-myc-ACE2 or pGFP-N3 plasmids (Invitrogen, Waltham, Massachusetts, USA). pGFP-N3 was employed as a positive control in the nucleofection and transfection protocols, and fluorescence was visualized with a Leica dMi8 fluorescence microscope (Leica Microsystem, Wetzlar, Germany).

For the nucleofection protocol, 1×10^6 of BEAS-2B cells were resuspended in 100 μL of Opti-MEM (Gibco, Waltham, Massachusetts, USA) with 5 μg of each plasmid, transferred to cuvettes and placed in the nucleofector. The chosen nucleofection program was strain-dependent. Then, cells were plated and incubated under standard conditions.

pCEP4-myc-ACE2 or pGFP-N3 were also transfected into A549 cells. For this, 2.5×10^5 cells were plated, incubated for 24 h and transfected with Opti-MEM containing previously mixed: lipofectamine 3000 (6 μL), P3000 (4 μL) and plasmid (2 μg). Then, the cells were incubated for 5 h, and the medium was replaced with DMEM-F12 supplemented with 10 % FBS.

Forty-eight hours after nucleofection or transfection, cells were expanded and selected with 125 ng/μL of the antibiotic hygromycin (Sigma) for 20 days. After selection, the cells were lysed with RIPA buffer, and total RNA was extracted with Trizol reagent (Invitrogen) to confirm ACE2 overexpression. Total RNA was quantified using a Nanodrop spectrophotometer and transcribed into cDNA with the High-Capacity kit. The cDNA obtained was subjected to RT-qPCR using the SYBR-Green reagent, primer pairs for Plasmid-ACE2 FW 5′-GGACC-CAGGAAATGTTCAGA-3′, RV 5′-CGTCCATTGTCACCTTTGTG-3′ and ROX. The reaction was carried out on an Applied 7500 RT-PCR machine. The analysis was performed by the relative comparison method ($2^{-\Delta\Delta CT}$) according to days of expansion. ACE2 expression was also assessed in lysed cells using an ELISA kit.

2.9. Statistical analysis

The results obtained were expressed as the mean ± SD (standard deviation). Data were evaluated first for normality using a Shapiro Wilk test, most of the variables were normally distributed, ($p > 0.05$). However, some variables were not, and they were transformed as log10. We used student's *t*-test, one-way analysis of variance (ANOVA) with Tukey's post-test for comparisons between three or more groups or Mixed-effects model (REML). The significance level was set at 5 % ($p < 0.05$). Statistical analyses were performed using GraphPad Prism version 8.0 (GraphPad Software, Inc., La Jolla, CA, USA). Sigma plot v13. (Systat, Palo Alto, CA, USA) was used to calculate the power of the test, only power > 0.8 was considered in the analysis. Principal component analysis (PCA) was conducted using normalized band intensity of the western blot experiments with Metaboanalyst v5.0.

3. Results and discussion

3.1. Kinetics of viral replication in cells

Undoubtedly, COVID-19 affects many organs, and, in some cases, yields long-lasting consequences [11]. Therefore, investigating SARS-CoV-2 infection in multiple cell lines can help generating a proposition that it can be further investigated in animal models and translated into human studies. Several authors have studied SARS-CoV-2 viral kinetics in various cell types [11,14]. However, it has been challenging to find an explanation for their susceptibility to the virus. Because of this, we had selected a panel of cell lines to determine the SARS-CoV-2 kinetics over time, classifying them according to their SARS-CoV-2 infection/replication capacity profiles. We used a qPCR assay for SARS-CoV-2 nucleocapsid protein (N) to evaluate the presence of genomic viral RNA during the replication cycle in each cell. BEAS-2B, A549, Caco-2, HEK293T, HuH7, Huvec, MCF7, SH-SY5Y, and Vero-E6 cells were infected with SARS-CoV-2 for 2 h to evaluate the initial viral uptake (Fig. 1A). This assay verified that the Vero-E6 and HuH7 showed virus internalization corresponding to 3×10^5 PFU/mL, 30-fold higher than BEAS-2B and 3–6 times higher than A549, Caco-2, HEK-293T, Huvec, MCF7 and SH-SY5Y cells (Fig. 1A).

Next, we evaluated the release of SARS-CoV-2 in the supernatant (Figure 1B1) and the intracellular replication kinetics in the cells (Fig. 1B2). After 2 h of infection and removing excess non-internalized virus, all the cells were incubated for an additional 24, 48, 72 or 96 h to evaluate viral replication over time. Vero-E6 exhibited the highest virus levels in the supernatant, 8.4×10^8 PFU/mL, 72 hpi, a 3-log increase compared to the 24 hpi time point ($p < 0.0001$, Fig. 1B1). As shown in Fig. 1B2, intracellular viral accumulation occurred in shorter intervals with a peak at 48 hpi (2-log difference between 24 and 48 hpi, $p < 0.0001$). High virus levels in the supernatant were also observed in the HuH7 cell culture (Fig. 1B1). Moreover, despite a relatively lower intracellular viral load over time in HuH7cells, the extracellular viral load was 1.7×10^8 PFU/mL, with a 3-log difference between 24 and 48 hpi ($p = 0.01$) (Fig. 1B2).

Caco-2 cells also presented a high intracellular viral load (3-log difference between 24 and 48 hpi, $p < 0.0001$) (Fig. 1B2), followed by a maximum viral load in the supernatant (5.2×10^7 PFU/mL) at 72 hpi ($p = 0.048$) (Fig. 1B1). Chu et al. also observed a 72 h extracellular peak in Caco-2 infected with SARS-CoV-2 [14]. The intracellular viral load observed in the MCF7 line showed an increase at 48 hpi ($p = 0.0017$) (Fig. 1B2); however, this difference was not observed in the supernatant (Fig. 1B1).

In HEK-293T and HUVEC cells, the peak of intracellular viral load was observed at 48 hpi ($p = 0.009$, Fig. 1B2) and 72 hpi, respectively (p

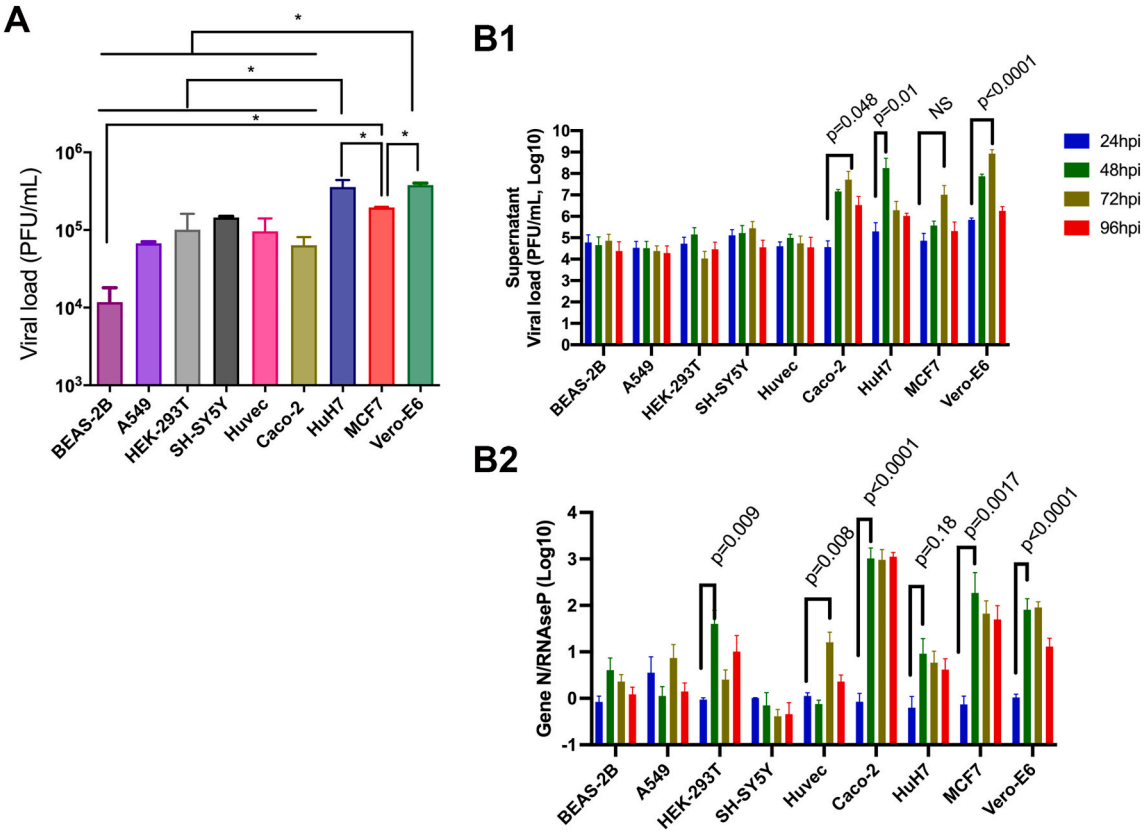

Fig. 1. SARS-CoV-2 kinetics in different cell types. A. Viral load 2 h post-infection (hpi) with SARS-CoV-2 ($n = 3$/group). One-way ANOVA followed by Tukey's test, $F(8,18) = 23.33$. B. SARS-CoV-2 extracellular (B1) and intracellular (B2) viral loads in different cell lines over time (n = 3–4/group). *$p < 0.05$. NS: non-significant. Mixed-effects model (REML) followed by Tukey's test, $F(8,27) = 8.96$ (B1), $F(8,87) = 32.9$ (B2).

= 0.008, Fig. 1B2). However, no difference was observed in the supernatant over time in either cell line. Chu et al. also observed a peak of SARS-CoV-2 replication in HEK-293T cells [14], which is in line with our results. Previously it was reported that Huvec cells are potentially vulnerable to SARS-CoV-2 [11], yet our results suggest these cells have similar viral replication properties as HEK-293 T cells. Interestingly, SH-SY5Y, a human neuroblastoma cell line widely used as a cell model of undifferentiated neurons, can also be infected by SARS-CoV-2 [15], albeit with a low viral replication profile. Based on these results, the Vero-E6, HuH7, MCF7 and Caco-2 cell lines displayed the highest viral replication capacities, followed by the other cell lines (BEAS-2B, A549, HEK-293T, HUVEC and SH-SY5Y) had a low viral replication capacity.

Several authors have studied SARS-CoV-2 viral kinetics in various cell types [11,14]. Hoffman et al. showed that SARS-CoV-2 entrance depends on ACE2 and TMPRSS2, the authors also observed that Vero-E6, Caco-2 and Calu-3 were highly permissive to the virus [11]. Similar results were also found by Chu et al. [14]. Our panel included several cell lines tested by Hoffman et al. and extended the virus infection from 24 to 96 h [11]. In another study, Kumar et al. analyzed 17 literature databases to produce a systematic review assessing the compatibility of cell types to SARS-CoV-2 infection [8]. This review showed that the most frequently used cells, including Vero E6, HEK293, HuH-7, Calu-3, and Caco-2 cells, are permissive to virus infection, have good replication rates and are easy to maintain in culture. In the present study, we have included BEAS-2B and A549, because they are frequently used as a model for pulmonary studies and are easier to cultivate, compared to Calu-3. We also decide to study vascular (Huvec), neuronal (SH-SY5Y) and glandular (MCF7) cell lines, due to the severity of infection on these tissues.

Since pandemic started, several studies have clarified that COVID-19

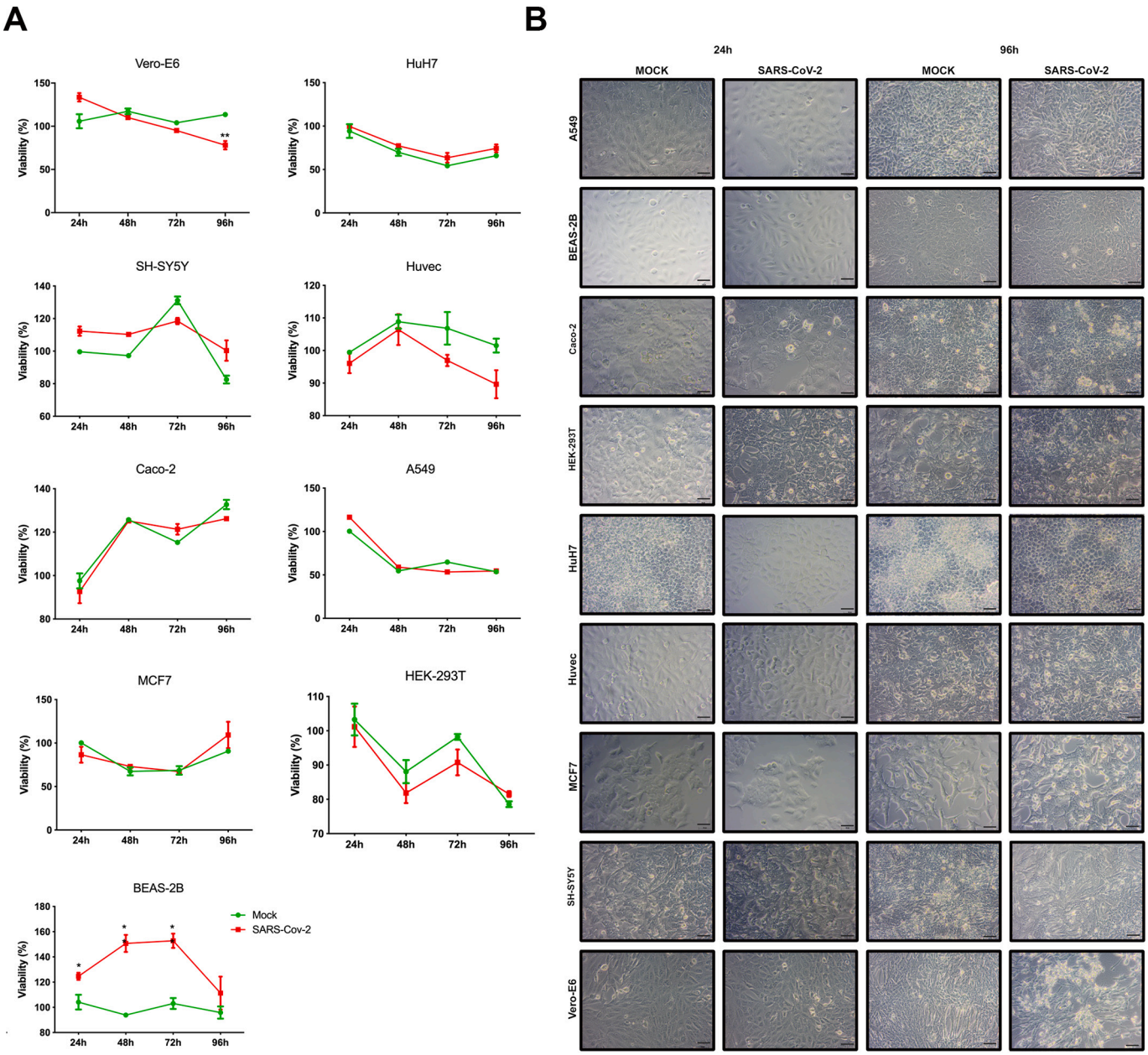

Fig. 2. Cell viability after SARS-CoV-2 infection. A. Cell viability assessed in the presence or absence of SARS-CoV-2 over time ($n = 3$). Two-way ANOVA, followed by Tukey's post-test. $^{**}p < 0.001$ and $^{*}p < 0.05$. F(3,6) = 32.86 (Vero-E6), 0.63 (HuH7), 19.4 (SH-SY5Y), 0.68 (Huvec), 0.82 (Caco-2), 297.8 (A549), 5.48 (MCF7), 5.83 (HEK-293 T), 3.59 (BEAS-2B). B. Representative images were taken 24 h and 96 h in the presence (red) or absence (green) of SARS-CoV-2. Mock (non-infected cells). Scale bar: 50 μm. (For interpretation of the references to colour in this figure legend, the reader is referred to the web version of this article.)

produced,not only a respiratory syndrome, but also a systemic disorder with consequences to all human systems. Libby & Lüscher proposed that COVID19 would be an "endothelial disease" associated with oxidative stress, inflammation and myocarditis [16]. SARS-CoV-2 can change the cells' protein levels, a recent study conducted by Duer et al., showed increased levels of troponin-t after SARS-CoV-2 infection, this would be associated with the inability of the heart to accommodate high viral load combined with a decrease in systemic oxygenation, and electrolyte variance causing additional stress on the compromised heart [17].

Ashraf et al. and Gavriatopoulou et al. reviewed publications related to organ invasiveness and ACE2, raising the question about how COVID-19 promotes neurological, skin, and kidney alterations, among others, making it a broad-spectrum disease [18,19]. Many factors, including infectivity (expression of receptors), metabolic rate, and resistance to cell death (cytopathic effect), can lead a cell to become a good producer of SARS-CoV-2. Thus, our next step was to evaluate the cytopathic effect promoted by the virus.

3.2. Metabolic effects on cell types and viability

The cytopathic effect promoted by the virus is evidenced by the formation of plaques, which is indicative of cell death. Plaques were only observed in infected Vero-E6 cells (data not shown) and accompanied by a concomitant reduction of formazan formation over 96 h (Fig. 2A). This result indicates that as the infection and replication progressed, the infected culture had fewer viable cells than the uninfected culture. Concerning HuH7, MCF7, SH-SY5Y, HUVEC, HEK-293T, Caco-2, and A549 cell lines, no statistically significant changes in viability were detected between the infected groups and the Mock groups at each time point. Interestingly, the infected BEAS-2B cell line formed formazan at faster rates in the initial time points after infection (24 and 48 h), suggesting higher cell viability/proliferation levels in the early infection phases that are not sustained.

HEK-293 T kidney cell line, one of the main organs affected after viral infection [20], displayed a lower metabolism/viability profile than HuH7 cells and exhibited a larger cytopathic effect. Previously, it was reported that HUVEC cells are potentially vulnerable to SARS-CoV-2 [11], yet our results suggest that these cells have similar viral replication properties as HEK-293T cells. The metabolic rate seems crucial to HuH7, which displayed higher MTT assay values during the 96-h experimental protocol without a clear cytopathic effect. Importantly, this hepatocarcinoma-derived cell line was reported to have a massive loss of heterozygosity. Indeed, a particularly interesting mutation in p53 (TP53 p.Tyr220Cys) [21] is highly pathogenic (https://www.ncbi.nlm.nih.gov/clinvar/variation/127819/). Therefore, HuH7 is possibly the best virus replication cell line due to its resistance to apoptosis, and, in the presence of p53 mutations, it could have a loss of cytopathic effect. This possibility requires future investigations. This possibility requires future investigations. The HuH7 cell line is well-studied in COVID-19 research, including proteomic analysis [22] and pathogenic pathways for coronaviruses infection [23]. In 2005, Freymuth et al. evaluated a comprehensive panel of respiratory viruses and concluded that HuH7 is an adequate model for coronavirus infection and replication [24]. These results could account for why the liver is an organ consistently affected by COVID-19, as reviewed by Marjot et al. (2021) [25] and Wang et al. [26].

The next step was to evaluate the cellular morphology of the infected cells. All strains in the study were infected with SARS-CoV-2 at an MOI of 0.2 and incubated for 24, 48, 72 and 96 h. At the end of each incubation time, cells were fixed with 4 % PFA, and images were captured using a brightfield microscope (Fig. 2B). The obtained images verified that the infected BEAS-2B did not show any morphological alterations or cell number differences compared to Mock cells at any incubation times, including 24 and 48 h (Fig. 2B). Thus, the observed difference in formazan levels 24 and 48 hpi in the MTT assay (Fig. 2A) is not due to cell death or proliferation but rather suggests increased NAD(*P*)H-dependent cellular metabolism in early periods of infection. On the other hand, the Vero E6 cell line showed cell morphology changes at 48 hpi, along with increased necrotic body formation that accumulated over time (48, 72 and 96 h), generating empty spaces between the cells (plates). The images of A549, Caco-2, HEK-293T, HuH7, HUVEC, MCF7, and SHSY5Y cells are presented in Fig. 2 and do not reveal morphological or cell count differences between the control and infected groups regardless of the incubation time.

3.3. Differential SARS-CoV-2 receptor expression

It was previously shown that ACE2 and TMPRSS2 are important for SARS-CoV-2 entry into host cells [11]. Since the expression of these proteins may be related to the differences in the viral load observed among the cell lines (Fig. 1), we analyzed ACE2 and TMPRSS2 expression by western blot and RT-qPCR (Fig. 3). No significant differences in ACE2 protein levels were detected among the cell lines, except for BEAS-2B, which presented the lowest ACE2 expression (Fig. 3A1 and A2, $p < 0.05$). In line with this, previous publications have shown that the number of gene or protein expressions of ACE2 in the airways is low [27]. The MCF7 cells presented significantly higher ACE2 mRNA expression than A549, HEK-293T, HUVEC, Caco-2, HuH7 and Vero-E6 cells (Fig. 3C).

Since ACE2 is an enzymatic receptor, we also investigated the ACE2 activity in the cells. As shown in Fig. 3D, the Vero-E6 displayed the highest ACE2 activity among all cell lines. The HEK-293T cells also had elevated ACE2 activity compared to the other lines. In contrast, the A549, SH-SY5Y and HUVEC cell lines had lower ACE2 activity and were classified as having a low replicative capacity for SARS-CoV-2 replication (Fig. 1B1). ACE2 is a component of the renin-angiotensin system, which is responsible to degrade the vasoconstrictor angiotensin (Ang) II to the vasodilator Ang-(1-7) [28]. This enzyme is highly expressed in the kidney proximal tube [28]; thus it was expected that HEK-293T cells presented a higher activity of ACE2.

Measurements of TMPRSS2 protein demonstrated that Vero-E6 cells expressed the lowest quantity compared to all other cell types (Figure 3B1 and B2, $p < 0.05$). It is worth mentioning that because Vero-E6 cells are not from humans like the other cell lines, the reactivity between the antibody and target protein could be different. In agreement with this, previous publications showed that Vero-E6 cells, have low expression of TMPRSS2 and the SARS-CoV-2 entrance is mediated by cathepsin [29].

A549 cells presented lower TMPRSS2 protein levels than HEK293T, HUVEC and HuH7. Additionally, the A549 cell line has high expression levels in the subunit corresponding to 38 kDa, which was absent in the other cell lines (Fig. 3B1). Aguiar et al. reported several TMPRSS2 bands after immunoblotting in epithelial cell lines and also observed low levels of this protease in pulmonary cells [30].

TMPRSS2 mRNA expression was high in Caco-2, HuH7 and MCF7, cell lines with a high viral replication capacity (Fig. 3E). Thus, these data indicate that ACE2 and TMPRSS2 expression levels and/or activities are associated with, at least to some extent, each cell line's infection and replication rate.

The gene expression does not always correlate with protein. Thus, differences between protein and gene expression observed for ACE2 and TMPRSS2 would be explained by post-transcription modifications induced by miRNAs. Lambert et al. (2014) found that miR-421 was able to reduce ACE2 protein expression in HuH7 [31]. Kaur et al. also demonstrate that miR-32 modulates the expression of TMPRSS2 [32].

3.4. Evaluation of proteins related to autophagy flux, apoptosis and mitochondrial oxidative metabolism

Having revealed differential cell line-specific ACE2 and TMPRSS2 expression, we next sought to quantify the levels of proteins related to autophagic flux like microtubule-associated protein 1A/1B-light chain 3

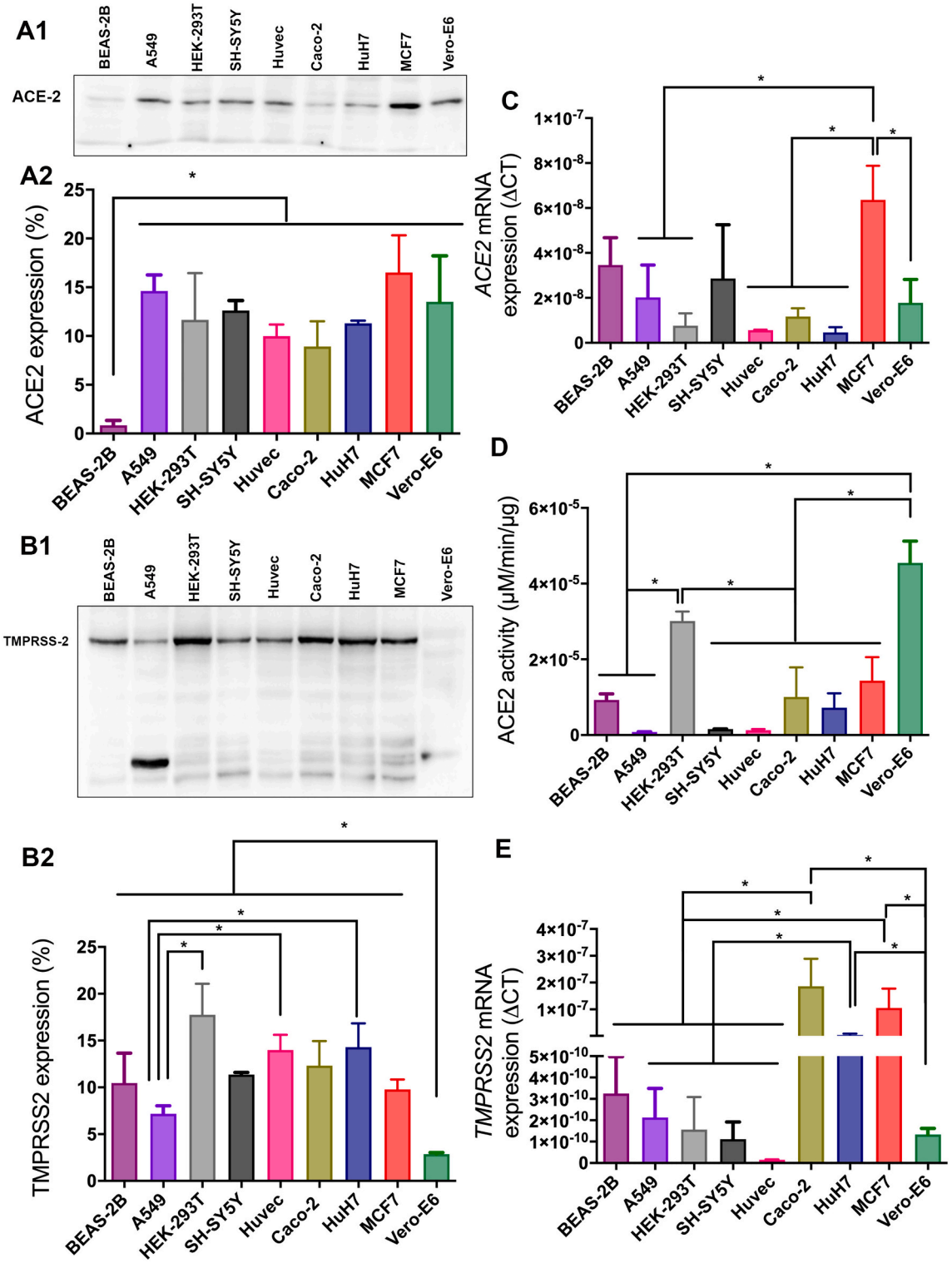

Fig. 3. Differential ACE2 and TMPRSS2 expression. A1. ACE2 expression according to Western blot analyses. $F(8,18) = 21.21$. A2. Histograms reporting the mean ± SD of ACE2 levels after normalization with the average intensity of the bands from three independent experiments. B1. TMPRSS2 expression according to Western blot analyses. $F(8,18) = 20$. B2. Histograms reporting the mean ± SD of TMPRSS2 levels after normalization with the average intensity of the bands from three independent experiments. C. *ACE2* mRNA expression according to RT-qPCR analyses. $F(8,18) = 6.09$. D. ACE2 activity. $F(8,18) = 26.34$. E. *TMPRSS2* mRNA expression according to RT-qPCR analyses. $F(8,18) = 43.22$. One-way ANOVA, followed by Tukey post-test. *$p < 0.05$. ($n = 3$/group).

phosphatidylethanolamine conjugate (LC3II) and lysosome-associated membrane glycoprotein 1 (Lamp-1). Previous studies have reported host autophagy flux involvement during SARS-CoV-2 infection [6,33,34]. Thus, since some studies demonstrated a direct effect of SARS-CoV-2 in autophagy induction [6,35] and autophagy-related compounds are of interest to COVID-19 research [33], we evaluated the basal autophagy levels and lysosomal enzymes involved in this process. As shown in Fig. 4A, cells with low viral replication profiles (e.g., A549 and HUVEC) presented higher LC3II levels compared to those with high viral replication profiles (e.g., HuH7 and MCF7) ($p < 0.05$).

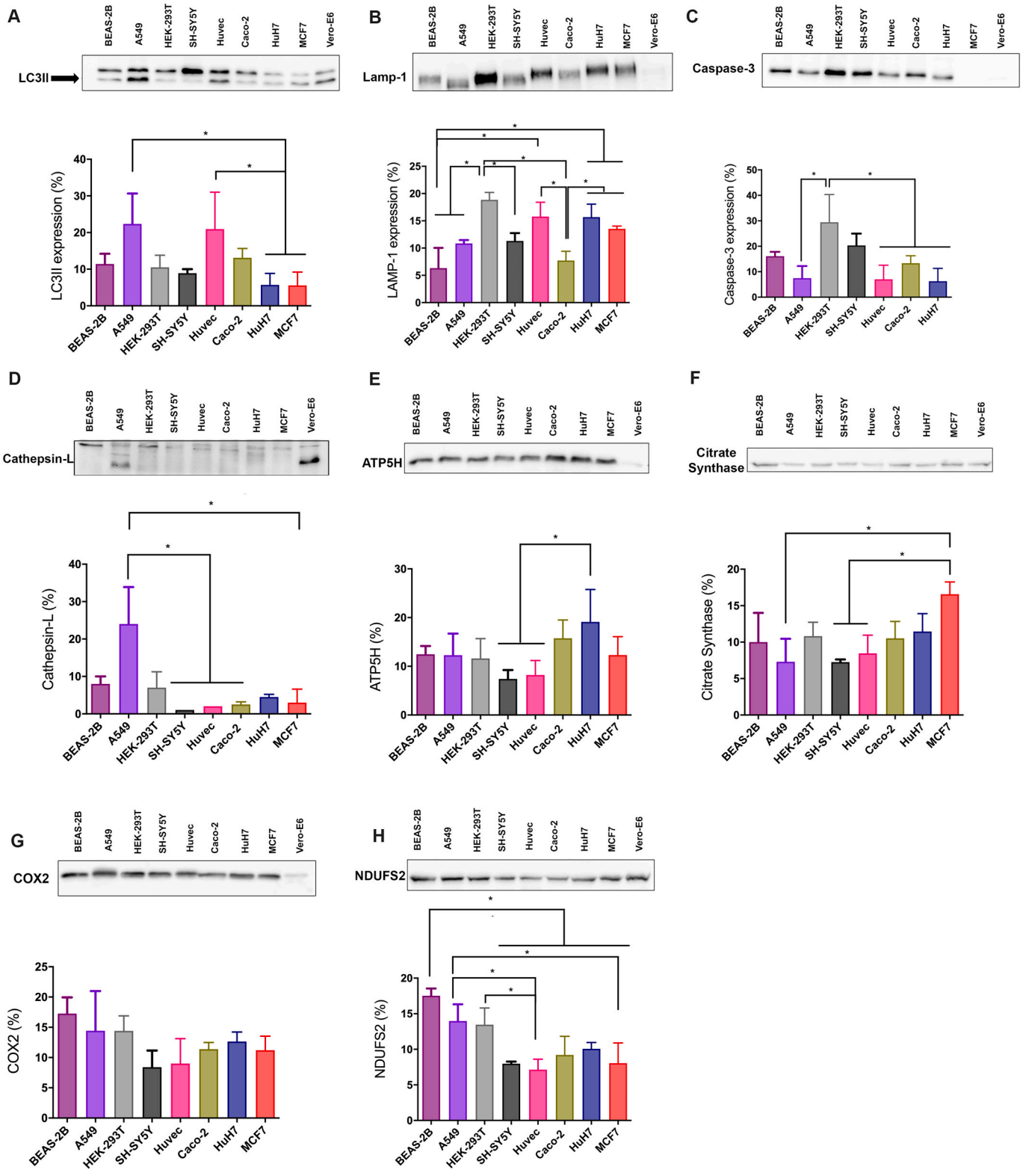

Fig. 4. Evaluation of proteins related to autophagy flux, apoptosis and mitochondrial oxidative metabolism. Protein levels were analyzed by Western blot, and histograms are reported as the mean ± SD of protein levels after normalization with the average intensity of the bands from three independent experiments. A. LC3-II, $F(8,15) = 4,2$. B. Lamp-1, $F(7,16) = 12.95$. C. Total caspase-3 total, $F(7,16) = 39.13$. D. Cathepsin-L, $F(8,10) = 9.1$. E. ATP5H, $F(8,17) = 12.73$. F. Citrate synthase, $F(8,16) = 2.26$. G. Cytochrome *c* oxidase subunit 2 (COX-2), $F(8,18) = 19.33$. H. NADH dehydrogenase iron-sulfor protein 2 (NDUFS2), $F(8,18) = 7.3$. One-way ANOVA, followed by Tukey's post-test. $^*p < 0.05$. ($n = 3$/group).

HUVEC cells also presented higher levels of Lamp-1 compared to Caco-2 and Beas-2B. HEK-293T, HuH7, and MCF7 Lamp-1 levels are similar to HUVEC (Fig. 4B). Interestingly, Caco-2, classified as a high viral replication profile, presented lower levels of Lamp-1 compared to HuH7 and MCF7, both classified as high profile. (Fig. 4B, $p < 0.05$). Therefore, it is unclear which mechanism is related to selective infectiveness in each cell group.

The expression of caspase-3, the principal effector of apoptosis, was upregulated in HEK-293T compared to A549, HUVEC, Caco-2 and HuH7 cells (Fig. 4C, $p < 0.05$). MCF7 presented indetectable levels of caspase-3. It was also determined that A549 cells had the highest cathepsin-L levels, a lysosomal cysteine protease (Fig. 4D, $p < 0.05$). Cathepsin-L has been reported to play a protective role against stress-mediated cell death [36] and is critical for SARS-CoV-2 infection [37].

Considering that cellular energy metabolism is important for sustainable SARS-CoV-2 replication [7], we next evaluated the level of proteins involved in mitochondrial metabolism in each cell line. Thus, we also evaluated proteins, including ATP synthase subunit d (ATP5H) (Fig. 4E), citrate synthase (Fig. 4F), COX2 (Fig. 4G) and NDUFS2 (Fig. 4H), which are involved in the electron transport chain, the main pathway for the ATP production. HuH7 displayed the highest levels of ATP5H, which was significantly different compared to SH-SY5Y and HUVEC (Fig. 4E, $p < 0.05$). Importantly, HuH7 was the cell line that presented the highest PFU/mL among human cell lines used in this study. In this sense, increased ATP synthase might metabolically support viral replication. Citrate synthase levels were highest in MCF7, with significantly augmented levels compared to A549, SH-SY5Y and HUVEC (Fig. 4F, $p < 0.05$). No differences were observed in the COX2 levels among the human cell lines (Fig. 4G). Concerning NDUFS2, BEAS-2B expressed higher levels of this protein compared to SH-SY5Y, HUVEC, Caco-2, HuH7 and MCF7 (Fig. 4H, $p < 0.05$). A549 and HEK-293 T also presented higher levels of NDUFS2 compared to HUVEC.

Since none of the individual proteins significantly correlated with intracellular or supernatant viral load, we evaluated whether multiple components could cluster the cell lines according to their replication capacity. We excluded the Vero-E6 cell line for this analysis because it is the only one derived from a nonhuman animal species, and different band intensities could have occurred due to the altered antibody reactivity.

When PCA was performed using all proteins evaluated in this study (ACE2, TMPRSS2, LC3, LAMP1, Cathepsin-L, caspase-3, ATP synthase, citrate synthase, COX2 and NDUFS2), we did not observe a clear separation between cell lines with high and low replication capacity (Fig. 5A). However, when the PCA was performed, including only proteins involved in energy production (i.e., ATP synthase, citrate synthase, COX2 and NDUFS2), cell lines with a high replication capacity (MCF7, Caco-2, HuH7) were clearly separated from those with lower replication capacities (Fig. 5B), suggesting that cellular energy metabolism is an important factor in replication capacity (Summarized in Fig. 6).

A previous study reported that mitochondrial metabolism was disturbed by SARS-CoV-2 infection, and enhanced mitochondrial permeability transition pore (PTP) activity has been observed upon the virus infection in human PBMCs [38]. In another report, a transcriptome databank of cell and clinical samples revealed that cellular respiration proteins and the complex I were downregulated by SARS-CoV-2 infection [39]. Moreover, Ajaz et al. analyzed the bioenergetics of PBMCs from patients with COVID-19 and identified that the mitochondrial energy function deficits could be compensated by an increase in glycolysis status [40]. According to the PCA results, metabolic proteins are the principal components that cluster cell lines according to replication capacity, with the highest including MCF7, HuH7 and Caco-2. Additionally, our data show that the cells which replicated more SARS-CoV-2 upregulate ATP production-related proteins. This possibility could be a critical factor for the selectiveness of the virus since viral replication in human cells requires substantial amounts of energy.

3.5. Overexpression of ACE2 changes the SARS-CoV-2 kinetics in pulmonary cells

After cell line characterization, the effect of ACE2 overexpression on the kinetics of SARS-CoV-2 replication was investigated. For this purpose, two pulmonary cell lines, BEAS-2B and A549, with low replication

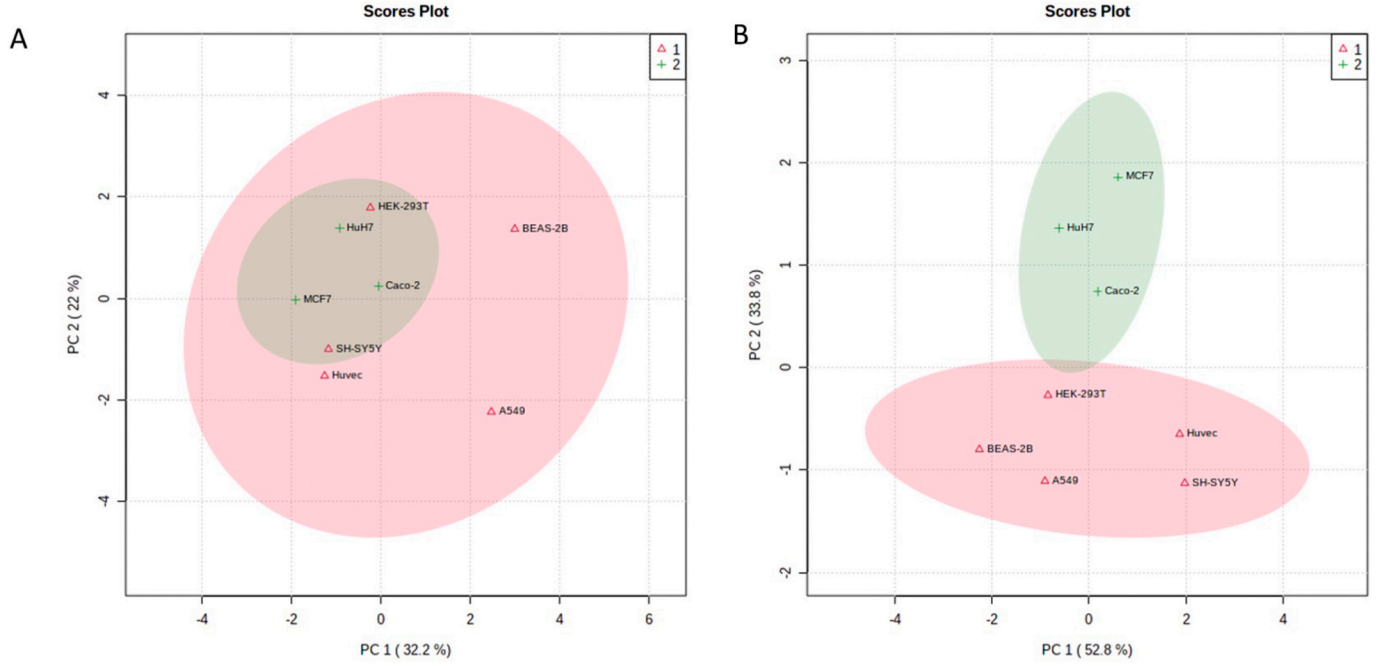

Fig. 5. PCA score plot was generated in Metaboanalyst v5.0 using A. ACE2, TMPRSS2, LC3II, LAMP1, Cathepsin-L, caspase-3, ATP synthase, citrate synthase, COX2, and NDUFS2, or B. ATP synthase, citrate synthase, COX2 and NDUFS2 (four proteins involved in energy metabolism). Green dots and clouds correspond to the cell lines with high replication capacity and 95 confidence intervals. Red dots and clouds indicate the cell lines with low replication capacity and 95 confidence intervals. (For interpretation of the references to colour in this figure legend, the reader is referred to the web version of this article.)

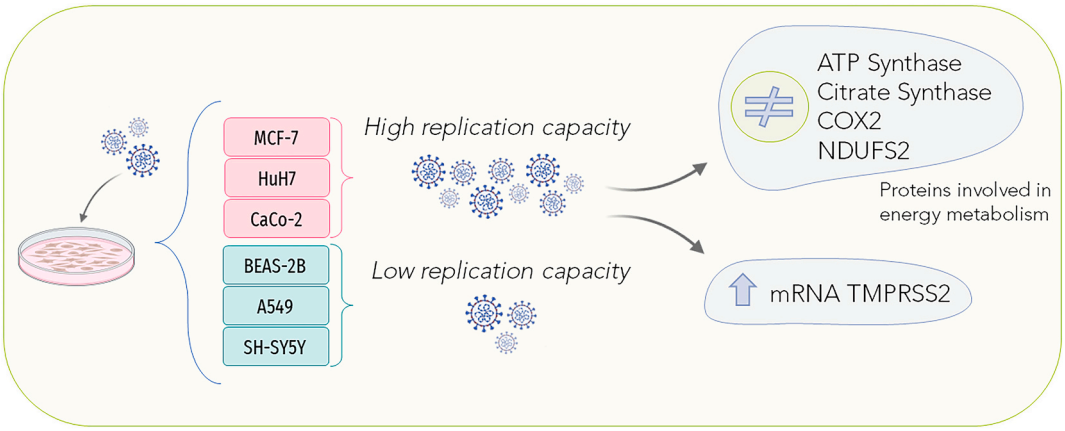

Fig. 6. Molecular mechanism related to SARS-CoV-2 replication. Created with Biorender.com

capacity, were selected. Long-term ACE2 overexpression was achieved in both cell lines for 30 days. However, after 45 days, the expression levels decreased to basal levels (Fig. 7A).

Two days after transfection, the expression of ACE2 was 103-fold higher in BEAS-2B-ACE2 compared to the control non-transfected cells. After 30 and 45 days, the expression levels decreased 61-fold (40 % reduction compared to the second-day post-transfection) and 28-fold (70 % reduction compared to the second-day post-transfection), respectively, but were still higher than non-transfected cells.

The A549-ACE2 cells presented a much higher ACE2 expression after two days (3400-fold) compared to the control. This expression was reduced to 1200-fold (65 % reduction compared to second-day post-transfection) and 35-fold (90 % reduction compared to second-day post-transfection) 30 and 45 days after transfection, respectively. The ACE2 protein level was 1.6-fold higher in A549-ACE2 than in BEAS-ACE2 30 days post-transfection (Fig. 7B). These results corroborate the study of Blanco-Melo et al. showing that ACE2 overexpression in A549 cells increases SARS-CoV-2 infectiveness [41].

Knowing that ACE2 is also an enzymatic receptor, the ACE2 activity was measured. In BEAS-ACE2, the ACE2 enzymatic activity was 83-fold higher than in BEAS-2B, and in A549-ACE2 cells, this activity was 400-fold higher than in control A549 cells (Fig. 7C). ACE2 activity was 24-fold higher in BEAS-2B than in A549 but was attenuated to 5-fold with ACE2 overexpression.

We next evaluated the effect of ACE2-overexpression on cell proliferation. The proliferation rate was decreased in both cell lines overexpressing ACE2 (Figs. 8A and B).

Finally, SARS-CoV-2 replication in both cell lines overexpressing ACE2 was evaluated (Fig. 9). Intriguingly, no significant difference in viral entry into the cells was observed at 2 hpi (Figs. 9 A and C) However, over time, the viral load accumulated in ACE2-overexpressing cells. The intracellular peak was reached at 48 hpi for A549-ACE2 (Fig. 9A) and BEAS-2B-ACE2 (Fig. 9C) and 72 hpi in the supernatant (Fig. 9B and D). It should be pointed out that the intracellular viral load peak was much higher for BEAS-2B-ACE2 (5683-fold) compared to A549-ACE2 (6-fold) cells. The same pattern was observed in the extracellular viral load for BEAS-2B-ACE (4×10^7 PFU/mL) and A549 (1.5×10^5 PFU/mL) at 72 hpi.

The in vitro models have the potential for investigating viral replication at different time scales. They are also important to test new drugs in development with antimicrobial effects [42]. In the present study, we successfully develop two pulmonary cell lines overexpressing ACE2 (Fig. 10), which would be used as a human cell model for pharmacological and molecular studies involving novel medicines for COVID-19.

4. Conclusions

The results herein presented indicate that the replication kinetics and infectivity of SARS-CoV-2 differ according to cell type. A panel of cell lines was selected to (1) determine viral kinetics over time, (2) classify cells based on their SARS-CoV-2 infection/replication capacity patterns and (3) evaluate gene and protein expression of TMPRSS2, ACE2 and other mitochondrial metabolic and autophagy-related proteins. Caco-2, MCF7 and HuH7 presented the highest viral load, which could be attributed both to the high levels of TMPRSS2 mRNA and to the different levels of ATP synthase, citrate synthase, COX2 and NDUSF2. Furthermore, ACE2 overexpression increased pulmonary cell SARS-CoV-2 replication capacity, making these cells a suitable model for in vitro pharmacology and mechanistic studies. The present study, therefore, has the potential to broaden the yet limited resources of SARS-CoV-2 infection studies, contributing to the establishment of adequate therapeutic approaches to COVID-19/contributing to the establishment of

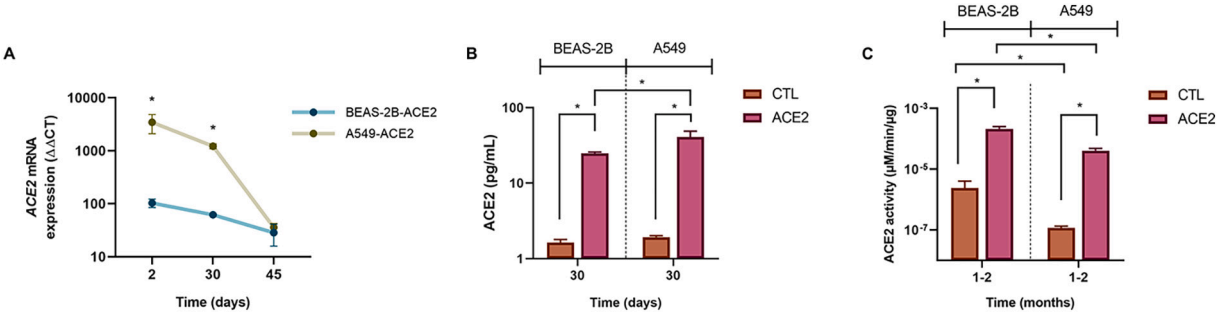

Fig. 7. ACE2 overexpression in pulmonary cells. A. Evaluation of ACE2 gene overexpression in BEAS-2B and A549 cells at 2, 30 and 45 days after nucleofection. F (2,4) = 6.8. B. ACE2 protein levels expression. F(3,8) = 64.94. C. ACE2 activity. F(3,14) = 229,3. Mixed effect model (REML), followed by Tukey's post-test. *$p < 0.05$.

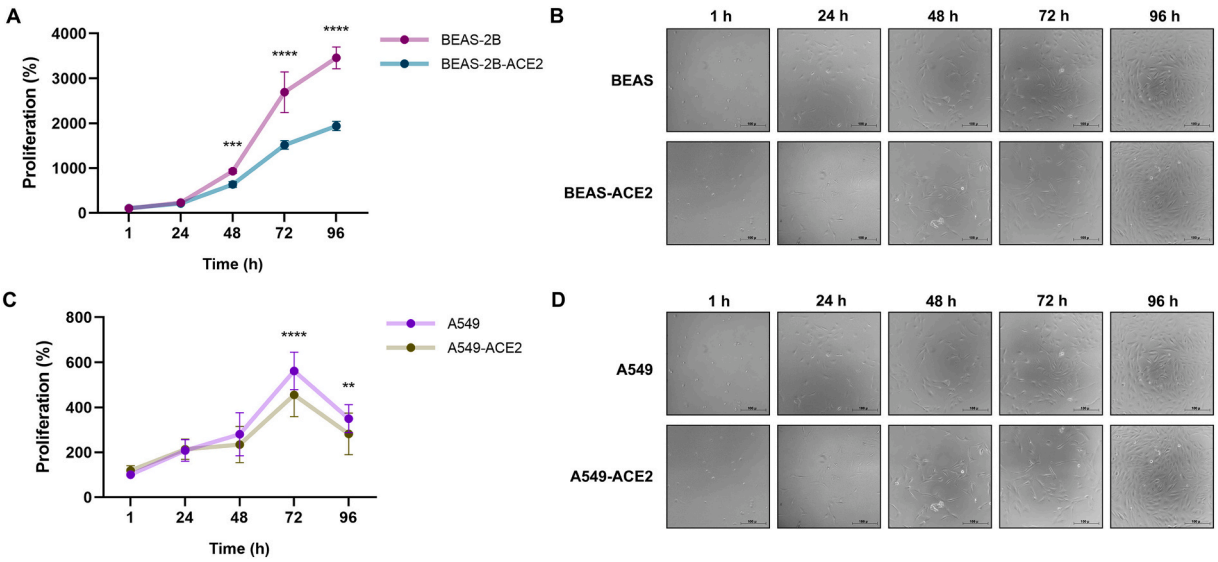

Fig. 8. MTT Cell proliferation assay with ACE2 overexpressing cells. Comparative evaluation of proliferation between BEAS-2B and BEAS-2B-ACE2 strains after 1, 24, 48, 72 and 96 h of incubation. A. and C. Graphical data plot analysis of the proliferation assay. $F(4,84) = 106.6$, $F(4,151) = 228.8$. B. and D. Representative images of cells overexpressing ACE2 versus control cells (20× magnification). Two-way ANOVA, followed by Sidak's post-test. *$p < 0.05$.

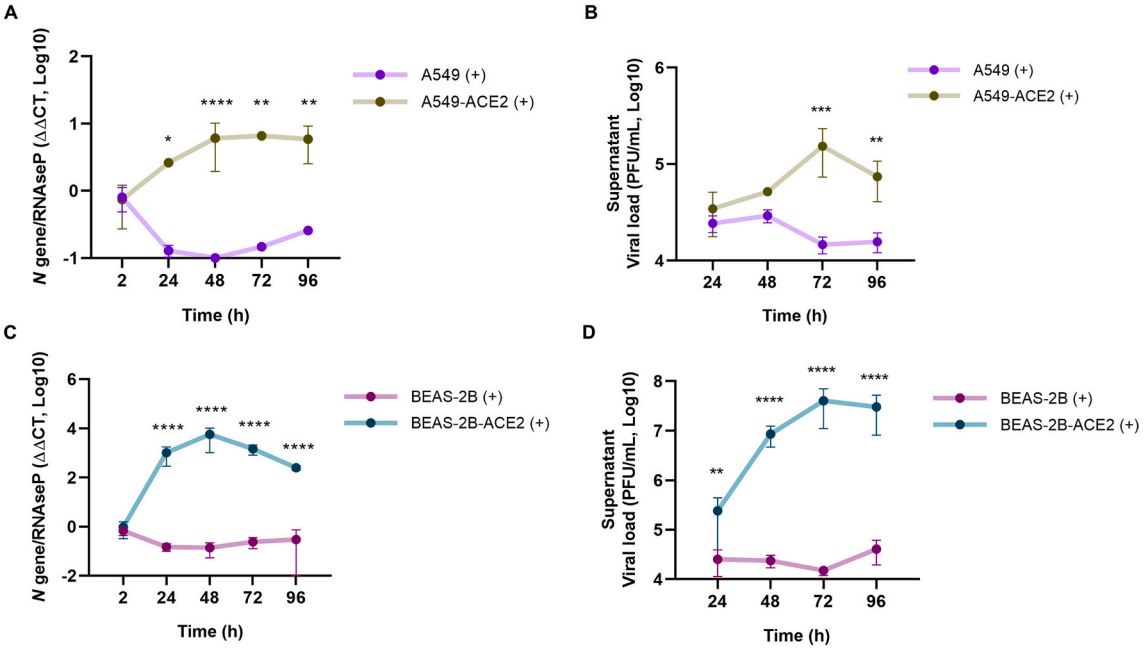

Fig. 9. ACE2 overexpression alters the viral load in pulmonary cells. Viral load 2, 24, 48, 72 and 96 h after SARS-CoV-2 infection with MOI 0.2. SARS-CoV-2 extracellular. A. and intracellular. B. replication over time in BEAS-2B and A549 cell lines overexpressing ACE2 versus controls. Mixed effect model (REML), followed by the Bonferroni post-test. *$p \leq 0.05$. $F(4,5) = 1.1$ (A), $F(3,6) = 8.72$, $F(4,34) = 60.23$ (C), $F(3,16) = 5.9$ (D).

solid scientific knowledge regarding COVID-19.

Supplementary data to this article can be found online at https://doi.org/10.1016/j.lfs.2022.120930.

CRediT authorship contribution statement

C.S.B and R.M.R.L: Investigation, Data Curation, Methodology, Writing - Original Draft. R.M: Investigation and Data Curation. G.C.P: Investigation and Data Curation. T.A.N and A.J.C: Investigation. R.M.B.M: Resources, Writing - Review & Editing. C.T.B: Investigation, data curation, Writing - Review & Editing. J.T.M: Conceptualization, Investigation, data curation, Writing - Review & Editing. L.M.R.J: Conceptualization, data curation, resources, Writing - Review & Editing. L.H.O: resources, Writing - Review & Editing. L.H.O: resources, Writing - Review & Editing. C.M.P, R.P.U and R.S.S: Conceptualization, data curation, resources, Writing – original draft, Review & Editing, supervision. All authors read and approved the final manuscript.

Funding

This work was supported by Fundação de Amparo à Pesquisa do Estado de São Paulo - FAPESP: 2016/20796-2 (RPU), 2020/04709-8 (RPU), 2020/13480-4 (CMP), 2020/06153-7 (RMRL), 2020/08943-5 (CTB, JTM. and LMRJ), 2006/60402-1 (RMB), 2019/10922-9 (RSS);

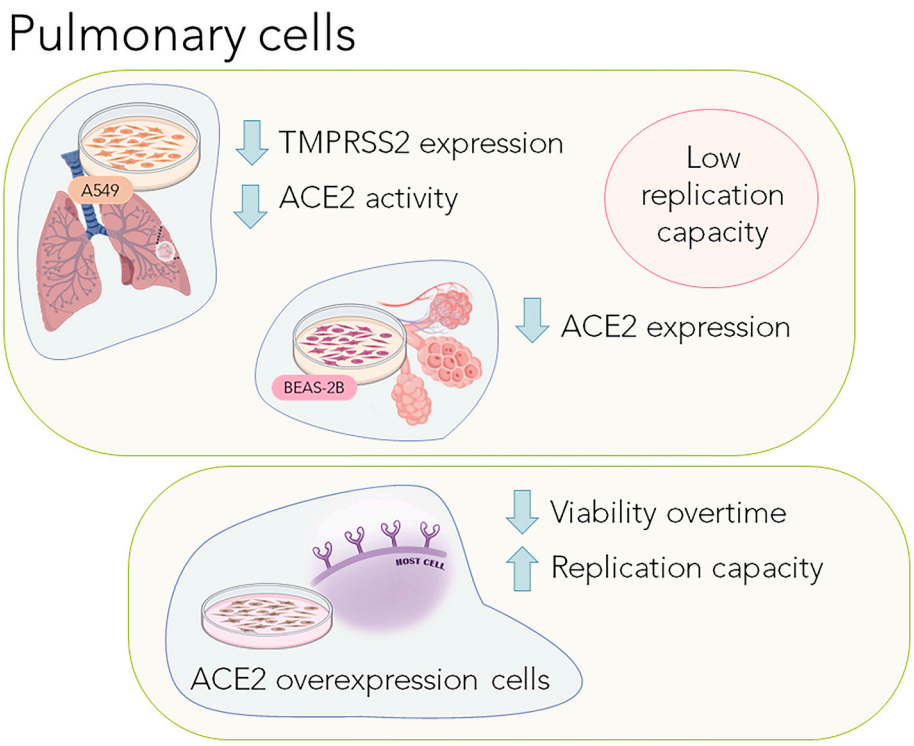

Fig. 10. ACE2 overexpression increased pulmonary cell SARS-CoV-2 replication capacity. Created with Biorender.com

Coordenação de Aperfeiçoamento de Pessoal de Nível Superior - CAPES: code 001 (CSB, TAN), Conselho Nacional de Desenvolvimento Científico e Tecnológico - CNPq: 303035/2018-8 (CMP), 405691/2018-1 (CTB); FAP-FCMSCSP 2021/2023.

Declaration of competing interest

The authors declare that there are no conflicts of interest.

Data availability

Data will be made available on request.

References

[1] S.A. Bhat F. Sher R. Kumar E. Karahmet S. Anam U. Haq A. Zafar E.C. Lima Environmental and health impacts of spraying COVID-19 disinfectants with associated challenges, (n.d.). doi:10.1007/s11356-021-16575-7.
[2] M.M. Lamers, B.L. Haagmans, SARS-CoV-2 pathogenesis, Nat. Rev. Microbiol. 20 (2022) 270–284, https://doi.org/10.1038/s41579-022-00713-0.
[3] M.L.G.A. Seixas, L.P. Mitre, S. Shams, G.B. Lanzuolo, C.S. Bartolomeo, E.A. Silva, C. M. Prado, R. Ureshino, R.S. Stilhano, Unraveling muscle impairment associated with COVID-19 and the role of 3D culture in its investigation, Front. Nutr. 9 (2022), 825629, https://doi.org/10.3389/fnut.2022.825629.
[4] S.A. Muhamad, A. Ugusman, J. Kumar, D. Skiba, A.A. Hamid, A. Aminuddin, COVID-19 and hypertension: the what, the why, and the how, Front. Physiol. 12 (2021), 665064, https://doi.org/10.3389/fphys.2021.665064.
[5] J. Yang, Y. Zheng, X. Gou, K. Pu, Z. Chen, Q. Guo, R. Ji, H. Wang, Y. Wang, Y. Zhou, Prevalence of comorbidities and its effects in coronavirus disease 2019 patients: a systematic review and meta-analysis, Int. J. Infect. Dis. 94 (2020) 91–95, https://doi.org/10.1016/j.ijid.2020.03.017.
[6] X. Hui, L. Zhang, L. Cao, K. Huang, Y. Zhao, Y. Zhang, X. Chen, X. Lin, M. Chen, M. Jin, SARS-CoV-2 promote autophagy to suppress type I interferon response, Signal Transduct. Target. Ther. 6 (2021), https://doi.org/10.1038/s41392-021-00574-8.
[7] P. Gatti, H.S. Ilamathi, K. Todkar, M. Germain, Mitochondria targeted viral replication and survival strategies—prospective on SARS-CoV-2, Front. Pharmacol. 11 (2020), https://doi.org/10.3389/fphar.2020.578599.
[8] S. Kumar, P. Sarma, H. Kaur, M. Prajapat, A. Bhattacharyya, P. Avti, N. Sehkhar, H. Kaur, S. Bansal, S. Mahendiratta, V.M. Mahalmani, H. Singh, A. Prakash, A. Kuhad, B. Medhi, Clinically relevant cell culture models and their significance in isolation, pathogenesis, vaccine development, repurposing and screening of new drugs for SARS-CoV-2: a systematic review, Tissue Cell. 70 (2021), https://doi.org/10.1016/j.tice.2021.101497.
[9] N.S. Ogando, T.J. Dalebout, J.C. Zevenhoven-Dobbe, R.W.A.L. Limpens, Y. van der Meer, L. Caly, J. Druce, J.J.C. de Vries, M. Kikkert, M. Barcena, I. Sidorov, E. J. Snijder, SARS-coronavirus-2 replication in vero E6 cells: replication kinetics, rapid adaptation and cytopathology, J. Gen. Virol. 101 (2020), https://doi.org/10.1099/jgv.0.001453.
[10] F.R. Cugola, I.R. Fernandes, F.B. Russo, B.C. Freitas, J.L.M. Dias, K.P. Guimarães, C. Benazzato, N. Almeida, G.C. Pignatari, S. Romero, C.M. Polonio, I. Cunha, C. L. Freitas, W.N. Brandaõ, C. Rossato, D.G. Andrade, D.D.P. Faria, A.T. Garcez, C. A. Buchpigel, C.T. Braconi, E. Mendes, A.A. Sall, P.M.D.A. Zanotto, J.P.S. Peron, A. R. Muotri, P.C.B.B. Beltrao-Braga, The Brazilian Zika virus strain causes birth defects in experimental models, Nature 534 (2016), https://doi.org/10.1038/nature18296.
[11] M. Hoffmann, H. Kleine-Weber, S. Schroeder, N. Krüger, T. Herrler, S. Erichsen, T. S. Schiergens, G. Herrler, N.H. Wu, A. Nitsche, M.A. Müller, C. Drosten, S. Pöhlmann, SARS-CoV-2 cell entry depends on ACE2 and TMPRSS2 and is blocked by a clinically proven protease inhibitor, Cell (2020), https://doi.org/10.1016/j.cell.2020.02.052.
[12] R.M.R. Lemes, A.J. Costa, C.S. Bartolomeo, T.B. Bassani, M.S. Nishino, S.S. Smaili, C.T. Braconi, E.F. da Cruz, A.L. Ramirez, J.T. Maricatto, L.M.R. Janini, C.M. Prado, R.S. Stilhano, R.P. Ureshino, G.J.da S. Pereira, R.M.de B. Maciel, 17β-Estradiol reduces SARS-CoV-2 infection in vitro, Physiol. Rep. 9 (2021), https://doi.org/10.14814/phy2.14707.
[13] C. Vickers, P. Hales, V. Kaushik, L. Dick, J. Gavin, J. Tang, K. Godbout, T. Parsons, E. Baronas, F. Hsieh, S. Acton, M. Patane, A. Nichols, P. Tummino, Hydrolysis of biological peptides by human angiotensin-converting enzyme-related carboxypeptidase, J. Biol. Chem. 277 (2002), https://doi.org/10.1074/jbc.M200581200.
[14] H. Chu, J.F.-W. Chan, T.T.-T. Yuen, H. Shuai, S. Yuan, Y. Wang, B. Hu, C.C.-Y. Yip, J.O.-L. Tsang, X. Huang, Y. Chai, D. Yang, Y. Hou, K.K.-H. Chik, X. Zhang, A.Y.-F. Fung, H.-W. Tsoi, J.-P. Cai, W.-M. Chan, J.D. Ip, A.W.-H. Chu, J. Zhou, D. C. Lung, K.-H. Kok, K.K.-W. To, O.T.-Y. Tsang, K.-H. Chan, K.-Y. Yuen, Comparative tropism, replication kinetics, and cell damage profiling of SARS-CoV-2 and SARS-CoV with implications for clinical manifestations, transmissibility, and laboratory studies of COVID-19: an observational study, Lancet Microbe 1 (2020), https://doi.org/10.1016/s2666-5247(20)30004-5.
[15] V. Bielarz, K. Willemart, N. Avalosse, K. De Swert, R. Lotfi, N. Lejeune, F. Poulain, N. Ninanne, J. Gilloteaux, N. Gillet, C. Nicaise, Susceptibility of neuroblastoma and glioblastoma cell lines to SARS-CoV-2 infection, Brain Res. 1758 (2021), https://doi.org/10.1016/j.brainres.2021.147344.
[16] P. Libby, T. Lüscher, COVID-19 is, in the end, an endothelial disease, Eur. Heart J. 41 (2020), https://doi.org/10.1093/eurheartj/ehaa623.
[17] G.D. Duerr, A. Heine, M. Hamiko, S. Zimmer, J.A. Luetkens, J. Nattermann, G. Rieke, A. Isaak, J. Jehle, S.A.E. Held, J.C. Wasmuth, M. Wittmann, C. P. Strassburg, P. Brossart, M. Coburn, H. Treede, G. Nickenig, C. Kurts, M. Velten,

Parameters predicting COVID-19-induced myocardial injury and mortality, Life Sci. 260 (2020), https://doi.org/10.1016/j.lfs.2020.118400.
[18] U.M. Ashraf, A.A. Abokor, J.M. Edwards, E.W. Waigi, R.S. Royfman, S.A.M. Hasan, K.B. Smedlund, A.M.G. Hardy, R. Chakravarti, L.G. Koch, Sars-cov-2, ace2 expression, and systemic organ invasion, Physiol. Genomics 53 (2021), https://doi.org/10.1152/physiolgenomics.00087.2020.
[19] M. Gavriatopoulou, E. Korompoki, D. Fotiou, I. Ntanasis-Stathopoulos, T. Psaltopoulou, E. Kastritis, E. Terpos, M.A. Dimopoulos, Organ-specific manifestations of COVID-19 infection, Clin. Exp. Med. 20 (2020), https://doi.org/10.1007/s10238-020-00648-x.
[20] S. Naicker, C.W. Yang, S.J. Hwang, B.C. Liu, J.H. Chen, V. Jha, The novel coronavirus 2019 epidemic and kidneys, Kidney Int. 97 (2020), https://doi.org/10.1016/j.kint.2020.03.001.
[21] F. Kasai, N. Hirayama, M. Ozawa, M. Satoh, A. Kohara, HuH-7 reference genome profile: complex karyotype composed of massive loss of heterozygosity, Hum. Cell 31 (2018), https://doi.org/10.1007/s13577-018-0212-3.
[22] N. Schmidt, C.A. Lareau, H. Keshishian, S. Ganskih, C. Schneider, T. Hennig, R. Melanson, S. Werner, Y. Wei, M. Zimmer, J. Ade, L. Kirschner, S. Zielinski, L. Dölken, E.S. Lander, N. Caliskan, U. Fischer, J. Vogel, S.A. Carr, J. Bodem, M. Munschauer, The SARS-CoV-2 RNA–protein interactome in infected human cells, Nat. Microbiol. 6 (2021), https://doi.org/10.1038/s41564-020-00846-z.
[23] J. Zhao, H. Zhou, W. Huang, J. Zhou, M. Qiu, Z. Deng, L. Chen, Y. Weng, L. Cai, Y. Gu, Q. Zheng, Q. Chen, X. Hou, L. Wang, L. Shen, Z. Yang, Cell morphological analysis of SARS-CoV-2 infection by transmission electron microscopy, J. Thorac. Dis. 12 (2020), https://doi.org/10.21037/jtd-20-1368.
[24] F. Freymuth, A. Vabret, F. Rozenberg, J. Dina, J. Petitjean, S. Gouarin, L. Legrand, S. Corbet, J. Brouard, P. Lebon, Replication of respiratory viruses, particularly influenza virus, rhinovirus, and coronavirus in HuH7 hepatocarcinoma cell line, J. Med. Virol. 77 (2005), https://doi.org/10.1002/jmv.20449.
[25] T. Marjot, G.J. Webb, A.S. Barritt, A.M. Moon, Z. Stamataki, V.W. Wong, E. Barnes, COVID-19 and liver disease: mechanistic and clinical perspectives, Nat. Rev. Gastroenterol. Hepatol. 18 (2021), https://doi.org/10.1038/s41575-021-00426-4.
[26] Y. Wang, S. Liu, H. Liu, W. Li, F. Lin, L. Jiang, X. Li, P. Xu, L. Zhang, L. Zhao, Y. Cao, J. Kang, J. Yang, L. Li, X. Liu, Y. Li, R. Nie, J. Mu, F. Lu, S. Zhao, J. Lu, J. Zhao, SARS-CoV-2 infection of the liver directly contributes to hepatic impairment in patients with COVID-19, J. Hepatol. 73 (2020), https://doi.org/10.1016/j.jhep.2020.05.002.
[27] I.T. Lee, T. Nakayama, C.T. Wu, Y. Goltsev, S. Jiang, P.A. Gall, C.K. Liao, L.C. Shih, C.M. Schürch, D.R. McIlwain, P. Chu, N.A. Borchard, D. Zarabanda, S.S. Dholakia, A. Yang, D. Kim, H. Chen, T. Kanie, C. Der Lin, M.H. Tsai, K.M. Phillips, R. Kim, J. B. Overdevest, M.A. Tyler, C.H. Yan, C.F. Lin, Y.T. Lin, D.T. Bau, G.J. Tsay, Z. M. Patel, Y.A. Tsou, A. Tzankov, M.S. Matter, C.J. Tai, T.H. Yeh, P.H. Hwang, G. P. Nolan, J.V. Nayak, P.K. Jackson, ACE2 localizes to the respiratory cilia and is not increased by ACE inhibitors or ARBs, Nat. Commun. 11 (2020), https://doi.org/10.1038/s41467-020-19145-6.
[28] F. Xiao, J. Zimpelmann, S. Agaybi, S.B. Gurley, L. Puente, K.D. Burns, Characterization of angiotensin-converting enzyme 2 ectodomain shedding from mouse proximal tubular cells, PLoS One. 9 (2014), https://doi.org/10.1371/journal.pone.0085958.
[29] A.Z. Mykytyn, T.I. Breugem, S. Riesebosch, D. Schipper, P.B. van den Doel, R. J. Rottier, M.M. Lamers, B.L. Haagmans, Sars-cov-2 entry into human airway organoids is serine protease-mediated and facilitated by the multibasic cleavage site, elife 10 (2021), https://doi.org/10.7554/ELIFE.64508.
[30] J.A. Aguiar, B.J.M. Tremblay, M.J. Mansfield, O. Woody, B. Lobb, A. Banerjee, A. Chandiramohan, N. Tiessen, Q. Cao, A. Dvorkin-Gheva, S. Revill, M.S. Miller, C. Carlsten, L. Organ, C. Joseph, A. John, P. Hanson, R.C. Austin, B.M. McManus, G. Jenkins, K. Mossman, K. Ask, A.C. Doxey, J.A. Hirota, Gene expression and in situ protein profiling of candidate SARS-CoV-2 receptors in human airway epithelial cells and lung tissue, Eur. Respir. J. 56 (2020), https://doi.org/10.1183/13993003.01123-2020.
[31] D.W. Lambert, L.A. Lambert, N.E. Clarke, N.M. Hooper, K.E. Porter, A.J. Turner, Angiotensin-converting enzyme 2 is subject to post-transcriptional regulation by miR-421, Clin. Sci. 127 (2014), https://doi.org/10.1042/CS20130420.
[32] T. Kaur, S. Kapila, R. Kapila, S. Kumar, D. Upadhyay, M. Kaur, C. Sharma, Tmprss2 specific miRNAs as promising regulators for SARS-CoV-2 entry checkpoint, Virus Res. 294 (2021), https://doi.org/10.1016/j.virusres.2020.198275.
[33] N.C. Gassen, J. Papies, T. Bajaj, J. Emanuel, F. Dethloff, R.L. Chua, J. Trimpert, N. Heinemann, C. Niemeyer, F. Weege, K. Hönzke, T. Aschman, D.E. Heinz, K. Weckmann, T. Ebert, A. Zellner, M. Lennarz, E. Wyler, S. Schroeder, A. Richter, D. Niemeyer, K. Hoffmann, T.F. Meyer, F.L. Heppner, V.M. Corman, M. Landthaler, A.C. Hocke, M. Morkel, N. Osterrieder, C. Conrad, R. Eils, H. Radbruch, P. Giavalisco, C. Drosten, M.A. Müller, SARS-CoV-2-mediated dysregulation of metabolism and autophagy uncovers host-targeting antivirals, Nat. Commun. 12 (2021), https://doi.org/10.1038/s41467-021-24007-w.
[34] W.I. Twu, J.Y. Lee, H. Kim, V. Prasad, B. Cerikan, U. Haselmann, K. Tabata, R. Bartenschlager, Contribution of autophagy machinery factors to HCV and SARS-CoV-2 replication organelle formation, Cell Rep. 37 (2021), https://doi.org/10.1016/j.celrep.2021.110049.
[35] H. Pan, G. Mostoslavsky, E. Eruslanov, D.N. Kotton, I. Kramnik, Dual-promoter lentiviral system allows inducible expression of noxious proteins in macrophages, J. Immunol. Methods 329 (2008) 31–44, https://doi.org/10.1016/j.jim.2007.09.009.
[36] X. Zheng, F. Chu, B.L. Mirkin, T. Sudha, S.A. Mousa, A. Rebbaa, Role of the proteolytic hierarchy between cathepsin L, cathepsin D and caspase-3 in regulation of cellular susceptibility to apoptosis and autophagy, Biochim. Biophys. Acta - Mol. Cell Res. 1783 (2008), https://doi.org/10.1016/j.bbamcr.2008.07.027.
[37] M.M. Zhao, W.L. Yang, F.Y. Yang, L. Zhang, W.J. Huang, W. Hou, C.F. Fan, R. H. Jin, Y.M. Feng, Y.C. Wang, J.K. Yang, Cathepsin L plays a key role in SARS-CoV-2 infection in humans and humanized mice and is a promising target for new drug development, Signal Transduct. Target. Ther. 6 (2021), https://doi.org/10.1038/s41392-021-00558-8.
[38] K. Ramachandran, S. Maity, A.R. Muthukumar, S. Kandala, D. Tomar, T.M. Abd El-Aziz, C. Allen, Y. Sun, M. Venkatesan, T.R. Madaris, K. Chiem, R. Truitt, N. Vishnu, G. Aune, A. Anderson, L. Martinez, W. Yang, J.D. Stockand, B.B. Singh, S. Srikantan, W.B. Reeves, M. Madesh, SARS-CoV-2 infection enhances mitochondrial PTP complex activity to perturb cardiac energetics, IScience 25 (2022), https://doi.org/10.1016/j.isci.2021.103722.
[39] B. Miller, A. Silverstein, M. Flores, K. Cao, H. Kumagai, H.H. Mehta, K. Yen, S. J. Kim, P. Cohen, Host mitochondrial transcriptome response to SARS-CoV-2 in multiple cell models and clinical samples, Sci. Rep. 11 (2021), https://doi.org/10.1038/s41598-020-79552-z.
[40] S. Ajaz, M.J. McPhail, K.K. Singh, S. Mujib, F.M. Trovato, S. Napoli, K. Agarwal, Mitochondrial metabolic manipulation by SARS-CoV-2 in peripheral blood mononuclear cells of patients with COVID-19, Am. J. Physiol. - Cell Physiol. 320 (2021), https://doi.org/10.1152/AJPCELL.00426.2020.
[41] D. Blanco-Melo, B.E. Nilsson-Payant, W.C. Liu, S. Uhl, D. Hoagland, R. Møller, T. X. Jordan, K. Oishi, M. Panis, D. Sachs, T.T. Wang, R.E. Schwartz, J.K. Lim, R. A. Albrecht, B.R. tenOever, Imbalanced host response to SARS-CoV-2 drives development of COVID-19, Cell 181 (2020), https://doi.org/10.1016/j.cell.2020.04.026.
[42] M. Maqsood, Z. Mushtaq, T. Rasheed, Z.U. Nisa, F. Sher, Thrombolytic and cytotoxic activity of different bioactive extracts of E. coli, Case Stud. Chem. Environ. Eng. 3 (2021), https://doi.org/10.1016/j.cscee.2021.100080.